

Energy Efficient Beamforming Training in Terahertz Communication Systems

Li-Hsiang Shen, *Member, IEEE*, Kai-Ten Feng, *Senior Member, IEEE*, Lie-Liang Yang, *Fellow, IEEE*

Abstract—Terahertz (THz) enables promising Tbps-level wireless transmission thanks to its prospect of ultra-huge spectrum utilization and narrow beamforming in the next sixth-generation (6G) communication system. Compared to millimeter wave (mmWave), THz intrinsically possesses compellingly severer molecular absorption and high pathloss serving confined coverage area. These defects should be well conquered under the employment of ultra-thin 3D beamforming with enormous deployed antennas with high beam gains. However, pencil-beams require substantially high overhead of time and power to train its optimal THz beamforming direction. We propose an energy efficient (EE) oriented THz beamforming (EETBF) scheme by separating the original complex problem into beamforming training (EETBF-BT) acquirement and learning-enabled training power assignment (EETBF-PA). The historical beam data is employed to update next beam selection policy. The performance results have demonstrated that the proposed EETBF outperforms the existing benchmarks leveraging full beam search, iterative search, linear/binary search as well as non-power-control based mechanism in open literature. Our proposed EETBF scheme results in the lowest training latency and power consumption, achieving the highest effective rate and EE performance.

Index Terms—THz, beam training, beamforming, power control, energy efficiency.

I. INTRODUCTION

With the proliferation of sixth-generation (6G) wireless communications, the tele-traffic demands are explosively escalating due to the emergence of novel applications such as X-reality, ultra-high definition images, and smart big-data [1]–[4]. As a paradigm shift from sub-6 GHz and millimeter wave (mmWave), terahertz (THz) [5], [6] ranging from 0.1 to 10 THz holds the promise of an abundant bandwidth capable of meeting the high data rate requirements of 6G, which attracts considerable attention due to its extremely-huge spectrum utilization. The first THz protocol is ratified by IEEE 802.15.3d [7] supporting ultra-wide band up to tens-of-GHz bandwidth at THz, which is applied in the potential stationery scenarios of wireless X-haul, data center, kiosk downloading, and intra-chip networks. Moreover, THz is also employed for mobility use cases [8]–[10], such as Internet of nano-mobile things, molecular and nano-sensor/communication mobile networks.

Most of the existing standards and applications focus on the frequency bands below 1 THz having cleaner channels and

lower signal losses [4], [11]. For example, IEEE 802.15.3d [7] standard operates at around 300 GHz, providing data rates up to 100 Gbps over short distances. These frequencies are ideal for applications in wireless backhaul, high-speed short-range communication, and imaging systems for security and medical purposes. The frequency band from 0.3 THz to 0.5 THz is adopted for ultra-high-speed communication for 6G development, enabling applications such as holographic projections and joint communication and sensing. The frequency band from 0.6 THz to 1 THz is also regarded as part of future 6G communications systems. The European Union’s Horizon 2020 programs [12], such as TeraNova and WORTECS, are exploring these frequencies for Tbps transmissions. However, the higher frequency bands from 2 THz to 3 THz, are not yet widely utilized for communication purposes. Instead, these frequencies are primarily applied in fields of spectroscopy and astronomy, where they are particularly suitable for scientific research, e.g., molecular physics and deep-space observations.

While, THz physical properties impose several implementation hurdles with respect to both the high power signal attenuation and detection, which requires advanced crafted THz beamforming techniques [5]. Due to much smaller wavelengths compared to mmWave, THz is capable of utilizing ultra massive multi-input-multi-output (UM-MIMO) [13]–[15] to generate narrow three-dimensional (3D) beams offering considerably-high antenna gains under miniaturized manufactured on-device space. Different from conventional mmWave networks, THz arises potential issues in physical and medium access control layers, including high-frequency channel modeling [16], molecular absorption modeling [17], pencil-beam orientation [18], and power consumption [14]. The current research papers primarily concentrate on evaluating the feasibility of THz beam-based channel measurement as shown in [18]–[20], combating the issues of short transmission distances. As an enhancement from conventional hybrid beamforming, the paper [14], [21] has rolled out an advanced beamforming from hardware architecture perspective, which employs array-of-subarrays with each carrying out different functionalities for spectrum- and energy-efficient (EE) solutions. Under such architecture, beam control becomes compellingly imperative. The authors in [22] have designed an appropriate long-term THz beam control for dynamic wireless power transfer in mobile nano-cells. In paper [11], an EE nano-node beam association is designed by considering the energy limitation and THz channel properties, whilst quality-of-service is additionally constrained in [23]. With the THz narrow-beam control, the paper [24] elaborates the benefits of spatial diversity of THz beamforming in non-orthogonal

Li-Hsiang Shen is with the Department of Communication Engineering, National Central University, Taoyuan 320317, Taiwan. (email: shen@ncu.edu.tw)

Kai-Ten Feng is with the Department of Electronics and Electrical Engineering, National Yang Ming Chiao Tung University (NYCU), Hsinchu 300093, Taiwan. (email: ktfeng@nycu.edu.tw)

Lie-Liang Yang is with the Department of Electronics and Computer Science, University of Southampton, Southampton SO17 1BJ, U.K. (e-mail: lly@ecs.soton.ac.uk)

multiple access. In [25], the authors have designed distance-aware adaptive THz beamforming, which manages system power and antenna subarray selection, i.e., beam selection. Other studies are exploring the usage of metasurfaces to enhance the coverage area of THz communications [26]–[28]. However, this induces additional expenditure in terms of further complex optimization of surface configuration and deployment, higher power consumption, and expenses related to manufacturing as well as maintenance. Moreover, the above-mentioned works of [11], [14], [22]–[28] are designed based on perfect beamforming, which neglect the overhead and defect of beamforming training before desirable data transmission [7], which potentially deteriorates the performance of pencil-beam-oriented THz systems.

In a generic protocol ratified by IEEE 802.11ad/ay [29], [30] for mmWave as well as in IEEE 802.15.3d [7] for THz, a frame, without loss of generality, is partitioned into two sessions, including beamforming training and data transmission durations. Excessive training overhead leaves little time for desirable data transfer, whilst overlength framing gives rise to outdated beam/channel information, especially in a short-distance THz network with mobility. In papers [26], [31], the authors have designed a hierarchical tree-based THz beam training or so-called iterative search, which is a more advanced mechanism compared to that in mmWave [32]. However, the global ground truth of narrow-beam index cannot be readily obtained owing to different beam patterns in a tree-based training. This has been well-addressed in the works of [29], [33], [34] by given a threshold guaranteeing adequate beam signal strength. Moreover, the initial stage of beamforming tree involves searching through wide beamwidths, which may inadvertently detect nearby nodes because of comparably low beam-gain as well as received power than narrow-beams. This situation has not been addressed or resolved in the papers of [26], [31], [33], [34]. In [7], exhaustive beam training is performed, which requires considerable overhead and potentially leaves no time for data transmission in a UM-MIMO enabled THz system. The authors in [35] have designed a low-overhead beam training method using detailed physical layer information. Similar concept in mmWave can be transferred to THz domain by employing only beam index and averaged signal strength at higher layers for massive beam training [36], [37]. To elaborate a little further, linear/binary beam search [38] is conventionally utilized but requiring frequent information feedback, whilst non-feedback based mobility-aware beamforming is conceived by [39]. However, most of the existing works in [7], [26], [31]–[35], [38] do not consider the compelling tradeoff among metrics of beam signal quality, beam alignment accuracy and training latency as well as throughput, which should be jointly designed as pointed out by [29]. In this context, high-efficiency THz beam training and alignment have been regarded as the highly challenging tasks, which should be considered when designing THz beamforming.

As previously explained, during beamforming training phase, weaker beams with low beam-gain can be compensated by extending the frame time, which may lead to a lack of time for data transfer. Moreover, all configured beams

may become infeasible impinged by environmental pitfall, regardless of the length of training frame. To mitigate this problem, we may utilize higher power during beamforming training to compensate for implausible beams. On the other hand, the energy can be preserved under sufficiently-strong beams, achieving high-EE training. Nevertheless, to the best of our knowledge, none of the existing works [7], [26], [29]–[39] have taken the dynamic power control into account during beamforming training. Instead, they always consume full-power, which potentially leads to energy wasting, weaker beams, and even unreachable signals. It is worth noting that the training power control is quite different from the instantaneous power allocation used for maximizing data transmission, as discussed in [11], [22], [24], [25]. During training, the power should be determined before acquiring information on either channels or beams, which is unknown and stochastic. This process substantially relies on probabilistic optimization as well as historical beamforming data [29]. Furthermore, with the rapid development of powerful machine and deep learning techniques, reinforcement learning has found to be in favour of solving complex problems in the dynamically-changing environments in the fields of wireless communications and networking [40]–[43]. In reinforcement learning [44], an agent interacts with the environment and updates the model based on the corresponding rewards, which is potentially capable of achieving a long-term optimal policy. Therefore, by utilizing the historical beam results and incorporating the learning-assisted power control, we design a low-complexity EE-oriented THz beamforming approach, which substantially strikes a compelling tradeoff between latency and accuracy as well as effective throughput/EE. The contributions of this paper are summarized as follows.

- We have conceived joint power control and 3D beamforming training in the EE-oriented THz communication system. It is capable of adjusting the appropriate beams and power for improving EE performance, while satisfying the guaranteed signal quality, available power, allowable training duration and beam alignment accuracy.
- We propose an EE-oriented THz beamforming (EETBF) scheme, where the original complex problem is partitioned into two sub-problems, namely acquiring candidate 3D beamforming training (EETBF-BT) and enabling dynamic training power assignment (EETBF-PA) through reinforcement learning. The proposed EETBF tends to extend the training duration in the cases of low beam alignment, whilst it maintains the training power to ensure acceptable signal quality. Historical beam data is employed to update the subsequent beam policy. Moreover, initial beam selection is adopted based on the channel quality obtained from historical beams.
- We guarantee a polynomial time complexity with the aid of long-term learning optimization. The performance results have demonstrated that the proposed EETBF outperforms the existing benchmarks leveraging full beam search, iterative search, linear/binary search as well as the non-power-control based mechanism found in open literature. It achieves the lowest training latency and

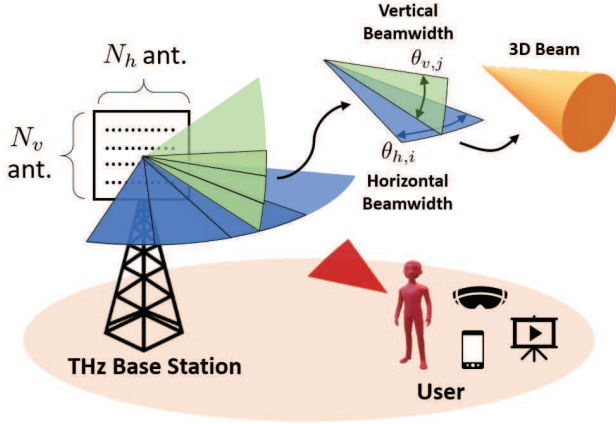


Fig. 1. Architecture of THz BS deployed with an antenna array having N_h horizontal and N_v vertical antenna elements. The corresponding beamwidths of the i -th horizontal and the j -th vertical beams are $\theta_{h,i}$ and $\theta_{v,j}$, respectively.

power consumption as well as the highest effective rate and EE performance.

The rest of this paper is organized as follows. In Section II, we present the THz system model, which includes beamforming, channel modeling, and beam training, followed by the problem formulation. The proposed EETBF approach adopting 3D beamforming training and learning-enabled training power control is elaborated in Section III. Performance evaluations of proposed EETBF scheme are conducted in Section IV. Finally, conclusions are drawn in Section V.

II. SYSTEM MODEL AND PROBLEM FORMULATION

A. Beamforming Model

As shown in Fig. 1, we consider a THz base station (BS) deployed with an antenna array with a total number of $N_t = N_h \cdot N_v$ antennas, where N_h and N_v denote the numbers of horizontal and vertical antenna elements, respectively. The THz BS located at $\mathbf{X}_{ap}(0, 0, h)$ is capable of conducting THz 3D beamforming to serve the desired moving user positioned at $\mathbf{X}_{ue}(x, y, z)$ within its serving coverage with the corresponding distance $d(t) = [x^2 + y^2 + (h - z)^2]^{1/2}$ between the THz BS and user. The beam profile is defined as the beam direction $\psi_{\mathcal{A},x}$ and beamwidth $\theta_{\mathcal{A},x}$, where $\mathcal{A} \in \{h, v\}$ denotes the horizontal and vertical beamforming directions, respectively, and the subscript $x = \{i, j\}$ indicates the index of either the i -th horizontal or the j -th vertical beam. It is noted that the THz beam is generated using full antennas to compromise the intrinsically severe path loss of THz transmissions. The beamforming gain of either horizontal or vertical beam direction is proportional to the configured number of antennas, where the THz beamforming gain can be asymptotically acquired as

$$G_{\mathcal{A}}(\theta_{\mathcal{A},x}, \psi_{\mathcal{A},x}) \approx \begin{cases} \frac{2\pi}{\theta_{\mathcal{A},x}}, & \text{if } |\psi_{\mathcal{A},x} - \tilde{\psi}_{\mathcal{A}}| \leq \frac{\theta_{\mathcal{A},x}}{2}, \\ \varepsilon, & \text{otherwise.} \end{cases} \quad (1)$$

From (1), we can infer that the THz mainlobe beam in the first expression of (1) is that the directional beam angle $\psi_{\mathcal{A},x}$

falls into the boresight angles $\tilde{\psi}_{\mathcal{A}}$ of the THz BS, which are acquired as $\tilde{\psi}_h = \tan^{-1}(y/x)$ and $\tilde{\psi}_v = \tan^{-1}(d/(z-h))$, respectively. The corresponding beamwidth is further computed as $\theta_{\mathcal{A},x} = 1.772\pi d_t/N_{\mathcal{A}}$, where d_t is the broadening factor determined by antenna spacing. Notation $\varepsilon \ll 1$ is a generalized constant gain for sidelobes. Note that the proposed system model can be theoretically extended to the bi-directional beams in both transmitter and receiver ends. However, considering practical cases, the user may only be equipped with a few antennas due to implementation issues. Therefore, we will neglect the receiving beamforming in the following discussions.

B. THz Channel

Inspired by [11], [17], [25], the distance-aware path loss of THz channel fading can be expressed as

$$H_{i,j}(t, f, d) = \rho_{i,j}(t) \left(\frac{c}{4\pi f d} \right)^2 e^{-\mathbb{K}_{THz}(f)d}, \quad (2)$$

where $\rho_{i,j}(t)$ is the small-scale variation of 3D beam (i, j) at time instant t , f is THz operating frequency, c is a constant of speed light, and $\mathbb{K}_{THz}(f)$ is the molecular absorption coefficient related to frequency. Notice that both the effects of line-of-sight (LOS) and non-light-of-sight (NLOS) THz channel can be asymptotically modeled by (2) [11]. As stated in [17], different THz channels will induce distinct coefficients of $\mathbb{K}_{THz}(f)$ based on the experimental measurement, which requires table mapping. We can readily observe from (2) that THz experiences additional absorption loss as decaying exponentially, which provokes compellingly high channel attenuation when compared to microwave and mmWave communications. Moreover, the environmental THz noise led by molecular perturbation is expressed as [17]

$$N(f, d) = k_B T_0 \left(1 - e^{-\mathbb{K}_{THz}(f)d} \right), \quad (3)$$

where k_B is the Boltzmann constant and T_0 is the reference temperature. It is worth mentioning that the noise model of (3) differs from that in micro/millimeter waves, since THz is substantially influenced by molecules alternating its native physical properties under different transmission distances [25].

C. THz Beamforming Training

In Fig. 2, we illustrate the beam training model and the corresponding framework. We can observe that the conventional beamforming training in Fig. 2(a) performs full-beam search as well as full-power training, which might lead to wasted energy and abundant training overhead. By contrast, in our proposed model shown in Fig. 2(b), we consider EE-oriented beam training, which relies on high power to compensate for low-quality beams and low power to preserve energy for strong beams. Moreover, partial beamforming training is conducted since some beams may become less informative. The overall procedure of beamforming training is demonstrated in Fig. 2(c). We consider that the THz-BS is configured with the available predefined codebook for THz 3D beam sector set of $\Phi = \{\Phi_h, \Phi_v\}$ with the candidate 3D beam training set of

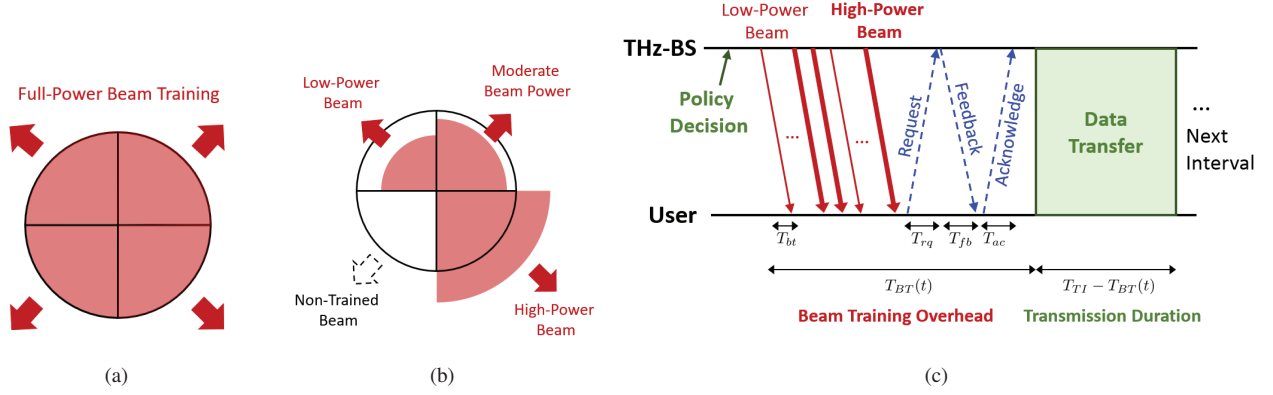


Fig. 2. The beam training model and framework. (a) Conventional full-power beam training. (b) Proposed EE-oriented beam training. (c) The designed protocol of THz beamforming training, including beam training overhead and transmission duration. Note that the policy decision is performed before initialization of beam training.

$\phi(t) = \{\phi_h(t), \phi_v(t)\}$ at the t -th interval. The BS is assumed to train a single 3D beam using a single time slot with the signal-to-noise ratio (SNR) of the (i, j) -th beam received by the user at frame t , which can be represented by

$$\gamma_{i,j}(t) = \frac{P_{i,j}(t)H_{i,j}(t, f, d) \cdot G_h(\theta_{h,i}, \psi_{h,i}) \cdot G_v(\theta_{v,j}, \psi_{v,j})}{N(f, d) + N_{NF}}, \quad (4)$$

where $\mathbf{P}(t) = \{P_{i,j}(t) | \forall i \in \phi_h(t), \forall j \in \phi_v(t)\}$ is the training power set, and N_{NF} indicates the power of additional noise figure from hardware devices. Based on the fundamental THz beamforming training process in [7] that is inherited from the similar concept in [29], the user will provide feedback on the received SNR $\gamma_{i,j}(t)$ to the THz BS with the optimal beam index as

$$k^*(t) = \{i^*(t), j^*(t)\} = \underset{i \in \phi_h(t), j \in \phi_v(t)}{\operatorname{argmax}} \gamma_{i,j}(t). \quad (5)$$

The BS will then store the optimal beam index $k^*(t) = \{i^*(t), j^*(t)\}$ with the corresponding SNR value of $\gamma_{i^*,j^*}(t)$. Owing to practical implementation of storage constraint, we assume that the THz-BS can store historical beam dataset from the past M -interval optimal beam indexes and corresponding SNR values, which is denoted as $\Xi(t, M) = \{k^*(t - \tau), \gamma_{i^*,j^*}(t - \tau) | \forall 1 \leq \tau \leq M\}$.

As for training overhead, we define T_{bt} as the duration of beam training for a single THz beam, which is followed by the request and feedback as well as acknowledgement phases with the respective durations of T_{rq} , T_{fb} and T_{ac} . We can therefore acquire the total overhead in terms of beamforming training latency at interval t , given by

$$T_{BT}(t) = |\phi(t)| \cdot T_{bt} + T_{rq} + T_{fb} + T_{ac}. \quad (6)$$

Consider that arbitrary beamforming training should be explicitly completed within a transmission interval T_{TI} , i.e., $T_{BT}(t) \leq T_{TI}$; otherwise, there will be no session for data transfer, leading to zero throughput. Based on the aforementioned definitions, the achievable effective throughput when

considering training overhead is expressed as

$$R(t) = W \cdot \max\left(0, 1 - \alpha(t)\right) \cdot \log_2\left(1 + \gamma_{i^*,j^*}(t) \mathbb{1}\{\gamma_{i^*,j^*}(t) \geq \gamma_{th}\}\right), \quad (7)$$

where W is the system bandwidth, and $\alpha(t) = T_{BT}(t)/T_{TI}$ is the ratio of THz beam training overhead. The $\max(\cdot, \cdot)$ prevents negative throughput, meaning that beam training duration exceeds the given transmission interval. In (7), the received SNR of the optimal beam is guaranteed to be higher than the predefined threshold of γ_{th} , which is regarded as the successful training, where $\mathbb{1}\{\cdot\}$ is an indicator function.

The averaged power consumption comprises both beamforming training and data transmission power which can be represented by

$$P(t) = \underbrace{\frac{1}{T_{TI}} \left(\sum_{i \in \phi_h(t)} \sum_{j \in \phi_v(t)} T_{bt} P_{i,j}(t) \right)}_{\text{Beam Training Power}} + \underbrace{(T_{TI} - T_{BT}) P_{i^*,j^*}(t)}_{\text{Data Transmission Power}}. \quad (8)$$

Therefore, the effective EE leveraging THz beamforming training latency in (6), rate performance in (7) and the power consumption in (8) can be acquired as

$$EE(t) = \frac{R(t)}{P(t)}. \quad (9)$$

Since THz communications are substantially affected by high path loss compared to microwave and mmWave, it becomes compellingly imperative to dynamically adjust the beamforming training power to achieve high EE, which however has not been considered in existing literature. Moreover, as the globally optimal beam may be unattainable, we accordingly characterize the averaged beam training alignment accuracy with acceptably-high SNR as

$$\xi(t) = \frac{1}{M} \sum_{\tau=0}^M \mathbb{1}\{\gamma_{i^*,j^*}(t - \tau) \geq \gamma_{th}\}. \quad (10)$$

D. Problem Formulation

Based on the above analysis, in this paper, our design aims at acquiring an appropriate policy of the beam training candidate set and corresponding training power under the maximization of the system effective EE and the consideration of joint beamforming training power, throughput, latency overhead, and beam alignment accuracy as follows:

$$\max_{\mathbf{P}(t), \phi(t)} EE(t) \quad (11a)$$

$$\text{s.t. } \gamma_{i^*, j^*}(t) \geq \gamma_{th}, \quad \forall i^* \in \phi_h(t), j^* \in \phi_v(t), t, \quad (11b)$$

$$\gamma_{i, j}(t) \geq \gamma_{dec}, \quad \forall i \in \phi_h(t), j \in \phi_v(t), t, \quad (11c)$$

$$P_{i, j}(t) \leq P_{be}, \quad \forall i \in \phi_h(t), j \in \phi_v(t), t, \quad (11d)$$

$$P(t) \leq P_{th}, \quad \forall t, \quad (11e)$$

$$T_{BI}(t) \leq T_{TI}, \quad \forall t, \quad (11f)$$

$$\xi(t) \geq \xi_{th} \quad \forall t. \quad (11g)$$

In the above problem, (11a) jointly considers the THz 3D beamforming training regarding the latency, throughput and power tradeoff. In this regards, we note that this is the first work jointly studying these issues. The beam signal is constrained by the trained optimal beam SNR in (11b), whereas all SNR values of training beams should be decodably higher than γ_{dec} in (11c). The allowable power P_{be} per beam direction is given in (11d) and the available total power of THz-BS P_{th} is provided in (11e). We also confine the allowable training time length in (11f) as well as the required beam alignment accuracy threshold ξ_{th} in (11g). We can infer from (11) that it consists of the mixed discrete integer and continuous variables, which give a nonlinear and non-convex problem. Moreover, the solution to the problem is intrinsically undetermined and stochastic, since the optimal beam performance is potentially unattainable until the completion of the full beamforming training procedure. Accordingly, we conceive to partition the problem into the beam selection and power assignment sub-problems by proposing the implementable schemes to approximately solve the EE maximization problem (11).

III. PROPOSED ENERGY EFFICIENT THZ BEAMFORMING (EETBF)

A. Proposed EETBF Scheme

Due to the non-convexity and nonlinearity in the EE problem (11), we partition it into two sub-problems, namely the beamforming training $\phi(t)$ of EETBF-BT and the power adjustment $\mathbf{P}(t)$ of EETBF-PA, where the corresponding BT and PA sub-problems are formulated as

$$\max_{\phi(t)} EE(t) \quad \text{s.t. (11b), (11c), (11f), (11g)}, \quad (12)$$

and

$$\max_{\mathbf{P}(t)} EE(t) \quad \text{s.t. (11b)–(11g)}. \quad (13)$$

According to the protocol designed in Fig. 2(c), the beam strength is unattainable until the completion of the whole training process. Therefore, the only information we have is the stored historical beam dataset of $\Xi(t, M)$, which is employed to obtain the optimal policy followed by power adjustment.

Algorithm 1: Proposed EETBF Scheme

- 1: Initialization:
 - 1) Configure THz BS 3D beam with horizontal/vertical beam set $\Phi = \{\Phi_h, \Phi_v\}$ and training beam set $\phi(t) = \{\phi_h(t), \phi_v(t)\}$
 - 2) Initialize training latency $T_{BT}(t)$, power consumption $P(t)$, throughput $R(t)$, alignment accuracy $\xi(t)$, and EE $E(t)$
 - 3) Set time counter $t = 0$
 - 2: **repeat**
 - 3: Transmission interval increment as $t = t + 1$
 - 4: **if** $t < M$ or insufficient accuracy $\xi(t) < \xi_{th}$ **then**
 - 5: Exhaustive beam training $\phi(t) = \Phi$
 - 6: Configure the maximum power $P_{i, j}(t) = P_{be}$
 - 7: **else**
 - 8: Perform Algorithm 2 to obtain horizontal and vertical beam training set $\phi(t) = \{\phi_h(t), \phi_v(t)\}$
 - 9: Conduct Algorithm 3 to acquire power allocation result $\mathbf{P}(t) = \{P_{i, j}(t) | \forall i \in \phi_h(t), \forall j \in \phi_v(t)\}$
 - 10: **end if**
 - 11: Obtain beamforming set $\phi(t)$ by spanning horizontal and vertical beam index sets $\{\phi_h(t), \phi_v(t)\}$
 - 12: THz BS executes 3D beamforming training employing beam policy $\phi(t)$ and power assignment $P_{i, j}(t)$
 - 13: User feedbacks the optimal beam indexed by $k^*(t) = \{i^*(t), j^*(t)\}$ in (5) with SNR $\gamma_{i^*, j^*}(t)$
 - 14: The THz BS stores the beam result in $\Xi(t, M)$
 - 15: Compute performances of training latency $T_{BI}(t)$, effective throughput $R(t)$, and EE $EE(t)$ given by (6), (7) and (9), respectively.
 - 16: Update Q-table in Algorithm 3
 - 17: **until** Termination of beamforming
-

The overall algorithm is elaborated as Algorithm 1. We require initialization of beam configuration Φ and $\phi(t)$, time counter t as well as performance indicators, such as latency, power consumption, throughput, beam alignment accuracy and EE. The exhaustive search with maximum power is conducted to initialize the dataset collection for M periods, whereas EETBF-BT/PA schemes are executed from the $(M + 1)$ -th interval. The details of both sub-schemes are elaborated in the following subsections.

1) *EETBF-BT*: Since 3D THz beamforming is considered, we should determine both the horizontal and vertical beam policies as $\{\phi_h(t), \phi_v(t)\}$. Inspired by [39], previous results may possess certain correlation with the current unknown and stochastic decision. Moreover, as shown in Algorithm 2, we independently process both dimensional beams and combine them finally by multiplying the two dimensions together. Given the historical beam dataset $\Xi(t, M)$ with window size M and SNR threshold γ_{th} , we can then derive the differences of beam index by $D_A = \text{diff}_A(\phi'(t))$, where historical optimal beam indexes are defined as $\phi'(t) = \{x^*(t - \tau) | \forall x = \{i, j\}, \tau = 1, 2, \dots, M\}$. We denote the search spanning size s_A indicating the number of timeslots of encompassing consecutive failures in previous beamforming training. If a worse beam with low SNR is acquired, i.e., $\gamma_{i^*, j^*}(t - \tau) \leq \gamma_{th}$ is regarded as the failure training in history, we iteratively enlarge the search size by $s_A = s_A + 1$. By contrast, we terminate to learn the central beam index as $\psi_A = \phi'(t - s_A)$ with a total spanning width $\varepsilon_A = s_A \cdot \max |D_A|$. In the followings, we

Algorithm 2: EETBF-BT

```

1: Initialization:
  1) Configure horizontal/vertical beam  $\Phi_{\mathcal{A}}, \phi_{\mathcal{A}}(t)$  where
      $\mathcal{A} = \{h, v\}$ 
  2) Given historical observation beam dataset  $\Xi(t, M)$  with
     window size  $M$ , SNR threshold  $\gamma_{th}$ 
2: Obtain historical optimal beam indexes
 $\phi'(t) = \{x^*(t - \tau) | \forall x = \{i, j\}, \tau = 1, 2, \dots, M\}$ 
3: Compute difference of beam index difference
 $D_{\mathcal{A}} = \text{diff}_{\mathcal{A}}(\phi'(t))$ 
4: Set spanning size  $s_{\mathcal{A}} = 1$ 
5: for  $\tau = 1, \dots, M$  do
6:   if  $\gamma_{i^*, j^*}(t - \tau) \leq \gamma_{th}$  then
7:     Increase size  $s_{\mathcal{A}} = s_{\mathcal{A}} + 1$  due to failure training in
     history
8:   else
9:     Learn central beam index  $\psi_{\mathcal{A}} = \phi'(t - s)$  and spanning
     width  $\varepsilon_{\mathcal{A}} = s_{\mathcal{A}} \cdot \max |D_{\mathcal{A}}|$  and terminate counting
10:  end if
11: end for
12: if  $\min D_{\mathcal{A}} \geq 0$  then
13:   Forward search as  $\phi_{\mathcal{A}}(t) = \{\psi_{\mathcal{A}}, \psi_{\mathcal{A}} + 1, \dots, \psi_{\mathcal{A}} + \varepsilon_{\mathcal{A}}\}$ 
14: else if  $\max D_{\mathcal{A}} < 0$  then
15:   Backward search as
      $\phi_{\mathcal{A}}(t) = \{\psi_{\mathcal{A}} - \varepsilon_{\mathcal{A}}, \psi_{\mathcal{A}} - \varepsilon_{\mathcal{A}} + 1, \dots, \psi_{\mathcal{A}}\}$ 
16: else
17:   Bi-directional search as
      $\phi_{\mathcal{A}}(t) = \{\psi_{\mathcal{A}} - \varepsilon_{\mathcal{A}}, \psi_{\mathcal{A}} - \varepsilon_{\mathcal{A}} + 1, \dots, \psi_{\mathcal{A}} + \varepsilon_{\mathcal{A}}\}$ 
18: end if
19: Output: Beam policy  $\phi_{\mathcal{A}}(t)$ 

```

Algorithm 3: EETBF-PA

```

1: Initialization:
2: (Training Power Acquisition)
3: Quantize power policy into  $Q$  levels
4: Randomize a small number  $\delta = [0, 1]$ 
5: if  $\delta \leq \delta_{th}$  then
6:   Randomize a power action  $a_t$  from discrete power set  $\mathcal{P}$ 
7: else
8:   Select optimal power action from Q-table as
      $a_t = \text{argmax}_{a'} Q(s_t, a')$ 
9: end if
10: Mapping power from action by  $P_{i,j}(t) = a_t \cdot P_{be}/Q$  and
     compute total power  $P(t)$  by (8)
11: if  $P(t) > P_{th}$  then
12:   Normalize individual power as  $P_{i,j}(t) = P_{i,j}(t) \cdot P_{th}/P(t)$ 
13: end if
14: Output: Training power assignment  $P_{i,j}(t)$ 
15: (Q-table Update)
16: Update current state by  $s_{t+1} = \mathcal{R} \left( \frac{R(t) \cdot s_Q}{R_{max}} \right)$ 
17: Update Q-table by  $Q(s_t, a_t) \leftarrow$ 
      $Q(s_t, a_t) + \eta_1 [EE(t) + \eta_2 \cdot \max_{a'}(s_{t+1}, a') - Q(s_t, a_t)]$ 

```

determine searching direction in three cases:

$$\phi_{\mathcal{A}}(t) = \{\psi_{\mathcal{A}}, \psi_{\mathcal{A}} + 1, \dots, \psi_{\mathcal{A}} + \varepsilon_{\mathcal{A}}\},$$

→ forward search if $\min D_{\mathcal{A}} \geq 0$, (14a)

$$\phi_{\mathcal{A}}(t) = \{\psi_{\mathcal{A}} - \varepsilon_{\mathcal{A}}, \psi_{\mathcal{A}} - \varepsilon_{\mathcal{A}} + 1, \dots, \psi_{\mathcal{A}}\},$$

→ backward search if $\max D_{\mathcal{A}} < 0$, (14b)

$$\phi_{\mathcal{A}}(t) = \{\psi_{\mathcal{A}} - \varepsilon_{\mathcal{A}}, \psi_{\mathcal{A}} - \varepsilon_{\mathcal{A}} + 1, \dots, \psi_{\mathcal{A}} + \varepsilon_{\mathcal{A}}\},$$

→ otherwise as bi-directional search. (14c)

Note that "forward/backward" indicates relative directions with the increment/decrement of horizontal and vertical beam indexes. In Fig. 3, we provide an example illustrating the beamforming training in (14). Note that here we only show the beam indexes in either horizontal or vertical dimension. We consider that the previous optimal central beam with its index given by $\psi_{\mathcal{A}} = 11$ and its corresponding search widths of $\varepsilon_{\mathcal{A}} = 4$. In Fig. 3(a), if $\min D_{\mathcal{A}} \geq 0$, we perform forward search and its beam training index set is given by $\{11, 12, 13, 14, 15\}$. If $\max D_{\mathcal{A}} < 0$ takes place, we execute backward search with the beam index set of $\{7, 8, 9, 10, 11\}$ in Fig. 3(b). In Fig. 3(c), the worst case of bi-directional search occurs when the above conditions are not satisfied, resulting in a beam search set of $\{7, 8, 9, \dots, 13, 14, 15\}$. After the completion of the beam index set determination in both dimensions, we proceed to combine both horizontal and vertical beam training sets. For example, as depicted in Fig. 3(d), we have determined the horizontal beam set $\{9, 10, \dots, 13, 14\}$ and the vertical one $\{7, 8, 9, 10\}$. Accordingly, the 3D beam training set is generated through combining the indexes from both dimensions.

2) *EETBF-PA*: For conventional optimization methods, the power assignment is conducted under known estimated channel information. Nonetheless, in the beam training case, no information is attainable except the historical outcomes. Consequently, the policy becomes undetermined and stochastic. Moreover, different beam directions potentially represent specific environmental conditions leading to difficulties in power adjustment. In this context, we employ reinforcement learning, as a long-term optimal policy, to intelligently and dynamically allocate the beamforming training power, which is elaborated in Algorithm 3. Note that the deep learning based reinforcement learning is deemed to be inappropriate for such implementation due to its high overhead of model training and unattainable input state of channel information. The important concept of reinforcement learning is the interaction between an agent and the environment, where an action a_t will be selected according to the resulting reward r_t and current state s_t in the established Q-table $Q(a_t, s_t)$. The reward is defined as a function of effective EE $r_t = EE(t)$. Furthermore, we define a quantized power set $\mathcal{P} = \{i \cdot P_{be}/Q | \forall 1 \leq i \leq Q\}$ with action $a_t = i$ denoted as an index of a single power solution, where we map the final power decision from action via

$$P_{i,j}(t) = a_t \cdot P_{be}/Q. \quad (15)$$

Notice that (15) implicitly fulfills the constraint in (11d) since the maximum power value occurs when $a_t = i = Q$, i.e., $P_{i,j}(t) = P_{be}$. If the total power is beyond the predefined budget in (11e), we conduct normalization utilizing $P_{i,j}(t) = P_{i,j}(t) \cdot P_{th}/P(t)$. Note that the state at the next interval $t+1$ is updated by leveraging the current rate result $R(t)$ as

$$s_{t+1} = \mathcal{R} \left(\frac{R(t) \cdot s_Q}{R_{max}} \right), \quad (16)$$

where $\mathcal{R}(\cdot)$ is the rounding operation, s_Q is the number of quantization level of states, and R_{max} is the maximum

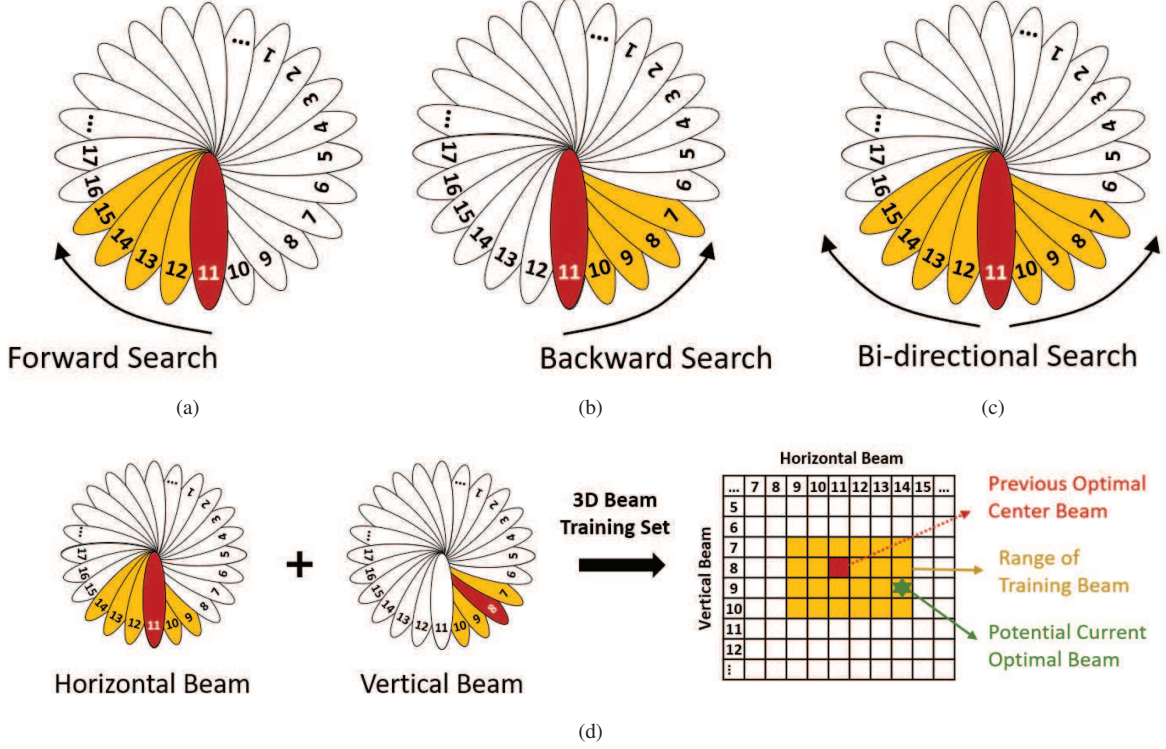


Fig. 3. Illustration of the beamforming training regarding (a) forward search in (14a), (b) backward search in (14b) and (c) bi-directional search in (14c). (d) The final 3D beamforming training set. Note that the beam with dark red indicates the previous optimal beam index ψ_A , whereas the beams with bright yellow represent the expanded search area calculated based on (14).

available rate from history, i.e., $R_{max} = \max R(t - \tau)$, $\forall 1 \leq \tau \leq M$. After the candidate beam acquirement in Algorithm 2, we adjust the training power by utilizing the greedy-based mechanism. When a randomized small number $\delta = [0, 1]$ is higher than a given threshold as $\delta > \delta_{th}$, we select the optimal power action from Q-table as

$$a_t = \operatorname{argmax}_{a'} Q(s_t, a'), \quad (17)$$

whilst a random action is chosen when $\delta \leq \delta_{th}$. Based on the training results in EETBF, we update the Q-table given by

$$Q(s_t, a_t) \leftarrow Q(s_t, a_t) + \eta_1 \cdot [r_t + \eta_2 \cdot \max_{a'} Q(s_{t+1}, a') - Q(s_t, a_t)], \quad (18)$$

where η_1 is the learning rate and η_2 indicates the discount factor. We can infer that (18) leverages both the current beamforming training EE and the potential power policy in the future.

B. Training Beam Initialization

We consider that a small amount of offline data for exhaustive beamforming is attainable for channel prediction during the initialization of online learning, which is shown in Algorithm 1, i.e., $t < M$ indicates insufficient data collection. From the history set of $\Xi(t, M)$, we can estimate the statistical

channel state information at the interval $t - \tau$ based on (4) as

$$H_{i,j}(t - \tau, f, d) = \frac{\gamma_{i,j}(t - \tau) \cdot \sigma^2}{P_{i,j}(t - \tau) \cdot G_h(\theta_{h,i}, \psi_{h,i}) \cdot G_v(\theta_{v,j}, \psi_{v,j})}, \quad \forall 1 \leq \tau \leq M, \quad (19)$$

where $\sigma^2 = N(f, d) + N_{NF}$. We employ a power-decaying function to predict the initial channel status rather than using average method due to the compelling significance of more recent data, which is represented by

$$\hat{H}_{i,j}(t, f, d) = \frac{1}{|\mathcal{H}|} \sum_{\tau=1}^M \beta^\tau \cdot H_{i,j}(t - \tau, f, d), \quad (20)$$

where $\mathcal{H} = \{H_{i,j}(t - \tau, f, d) \neq 0 | \forall 1 \leq \tau \leq M, i \in \Phi_h, j \in \Phi_v\}$ excludes the unpredictable channels due to potential blocking paths, and $0 < \beta < 1$ is the decaying factor. $|\mathcal{H}|$ means the amount of the collected channel information.

After obtaining the estimated beam channels, we now turn to tackle the constraints. We can infer that (11g) as beam alignment accuracy implies the similar meaning to that in (11b) and (11c). Therefore, we can rewrite (11b) and (11c) with alternative constraints respectively as

$$\max_{\forall i,j} P_{i,j}(t) \cdot \hat{H}_{i,j}(t, f, d) \cdot G_h(\theta_{h,i}, \psi_{h,i}) \cdot G_v(\theta_{v,j}, \psi_{v,j}) \geq \gamma_{th} \cdot \sigma^2, \quad (21)$$

$$P_{i,j}(t) \cdot \hat{H}_{i,j}(t, f, d) \cdot G_h(\theta_{h,i}, \psi_{h,i}) \cdot G_v(\theta_{v,j}, \psi_{v,j}) \geq \gamma_{dec} \cdot \sigma^2. \quad (22)$$

Note that the difference between these requirements is that

TABLE I
PARAMETER SETTING OF THZ

System Parameters	Value
BS Serving Radius	50 m
System Bandwidth W	1 GHz
Operating Frequency f	[0.1, 1] THz
Training power per beam P_{be}	15 dBm
Maximum Transmit Power P_{th}	27 dBm
Thermal Noise N_0	-174 dBm/Hz
Sidelobe Beam Gain ε	0.1
Transmission Interval	50 ms
Intervals of $T_{bt}, T_{rq}, T_{fb}, T_{ac}$	10 μ s
Quantization Level s_Q	100
Observation Window Size M	10
Random Action Probability δ_{th}	0.15
Learning Rate η_1	0.5
Discount Factor η_2	0.5
Decaying Factor β	0.95
User Velocity	{1.8, 10.8, 27} km/hr

the optimal beam should fulfill (21), whereas the other training beams must satisfy the decodability constraint of (22). Moreover, from (11f), we know that the maximum number of training beams should not exceed

$$N_{be} \triangleq |\phi(t)| = \frac{T_{TI} - T_{rq} - T_{fb} - T_{ac}}{T_{bt}}. \quad (23)$$

Based on (23), the top- N_{be} beams with the best possible channel quality in $\hat{\mathcal{H}} = \{\hat{H}_{i,j}(t, f, d) | \forall i \in \Phi_h, j \in \Phi_v\}$ are selected as the potential training candidates.

IV. PERFORMANCE EVALUATIONS

The system performance of proposed EETBF is evaluated through simulations. We evaluate the frequency bands from 0.1 to 1 THz, with the corresponding bandwidth of 1 GHz. The THz channel model in [11] is adopted. Note that the result in [11] implies that the higher frequency bands above 1 THz suffer from compellingly higher pathloss than those between [0.1, 1] THz. We set the thresholds of training beam SNR to $\gamma_{th} = 10$ dB and of the decodable SNR to $\gamma_{th} = 0$ dB. The training power per beam is set to $P_{be} = 15$ dBm, while the maximum total power consumption is set to $P_{th} = 27$ dBm. The time intervals are set equal to $T_{bt} = T_{rq} = T_{fb} = T_{ac} = 10 \mu$ s. The training duration should be smaller than $T_{TI} = [0.2, 1.2]$ s. Moreover, the training accuracy should be higher than $\xi_{th} = 0.7$. The remaining parameter settings are listed in Table I. We compare the proposed EETBF with and without training power control as well as the conventional full beam search with full power as baseline.

A. THz Characteristics

In Fig. 4, we study the beamforming requirement of beamwidths and antenna gains with respect to (w.r.t.) different numbers of THz antennas based on (4). Note that the perfect alignment of mainlobe beam is considered, i.e., the transmit beam angle $\psi_{A,x}$ falls into the boresight angles $\tilde{\psi}_A$ of the THz BS. We can infer that the beamwidth is inversely proportional to the number of antennas, whereas antenna gain

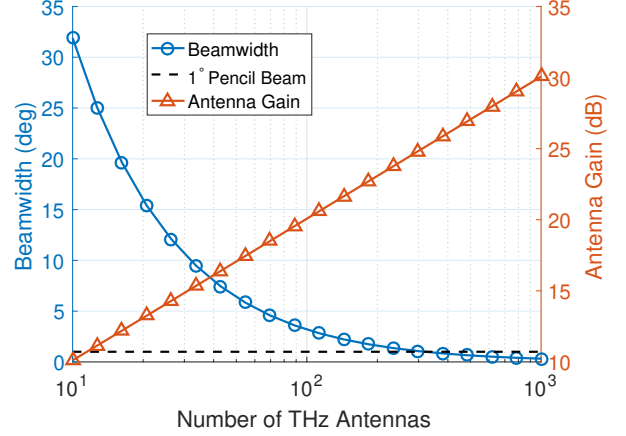


Fig. 4. The beamwidth and corresponding antenna gain w.r.t. different numbers of THz antennas.

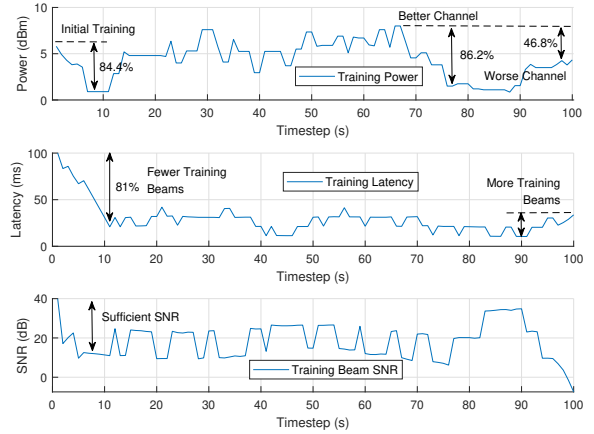


Fig. 5. Instantaneous performance of training power, latency and SNR values versus timesteps during the beamforming training process of the proposed EETBF scheme.

is linearly proportional to the number of antennas. That is, a smaller beamwidth can generate a higher beam gain, but more antennas are required for the beamforming. As shown in Fig. 4, 30 dB beamforming gain requires around a thousand antennas. Moreover, around 500 antennas are needed to form a 1° pencil-beam.

In Fig. 5, we analyze the instantaneous performances for different stages of beamforming training of the proposed EETBF scheme. We set the transmission interval to $T_{TI} = 1$ s for better observation. The training power, training latency, and the corresponding SNR values are studied. We can observe that the highest number of beams is required at the beginning owing to the initial training stage using exhaustive search. However, at a timestep of 10 s, EETBF can preserve 84.4% training power and reduce training latency by 81%. This is due to the fact that it requires fewer but more energy-efficient beams after learning the potential information of user trajectory. Moreover, an SNR of around 10 dB is attained for sufficiently decodable signals. When low-latency training is sustained under user mobility from 10 s to 65 s, EETBF

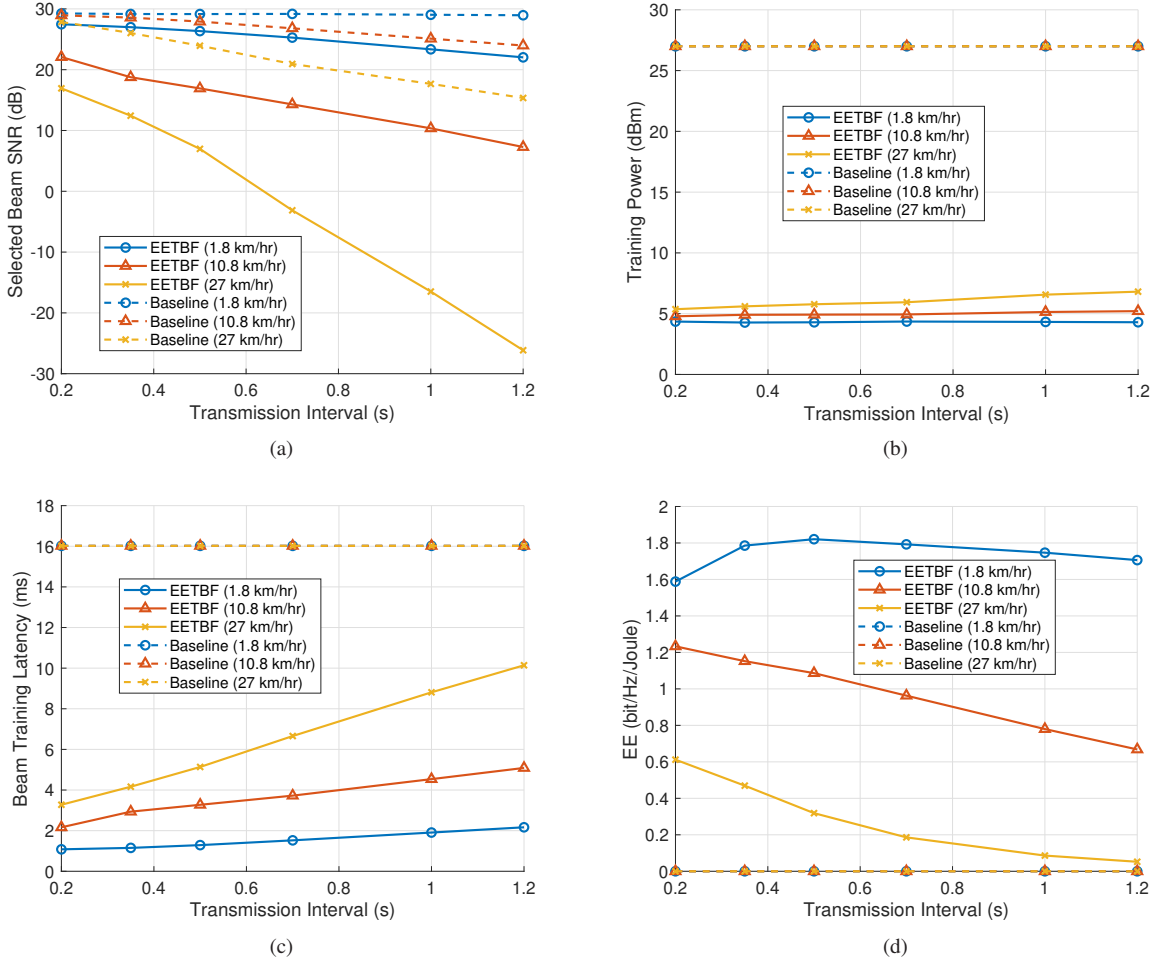


Fig. 6. Performance of EETBF compared to the baseline w.r.t. different velocity values of $\{1.8, 10.8, 27\}$ km/hr and transmission intervals $T_{TI} \in [0.2, 1.2]$ s. (a) Beam SNR (b) Training power (c) Training latency (d) EE.

potentially requires more power to compensate for weaker beams due to uncertain user movements. With better channel quality from the timestep of around 70 s to 90 s, around 86.2% of power can be preserved for high energy efficiency. However, from 90 to 100 s compared to that at 65 s, only around 46.8% of power is preserved under worse channel conditions. Such case also provokes more training beams involved for finding those with better signal quality.

B. Effect of Transmission Intervals

In Fig. 6, we investigate the performance of EETBF in comparison with the baseline schemes w.r.t. different velocity values of $\{1.8, 10.8, 27\}$ km/hr and transmission intervals of $T_{TI} \in [0.2, 1.2]$ s. It is worth mentioning that 1.8 km/hr simulates random pedestrian walk, whereas 10.8 and 27 km/hr are for vehicular speeds. Note that the baseline scheme considered is the conventional full beam search with full power during beam training. In Fig. 6(a), we can observe that a higher velocity induces a lower beam SNR, since faster movement potentially leads to the expired training beams. Furthermore, with longer transmission intervals, out-of-date beams also cause low SNR values, whereas shorter transmission intervals

can frequently refresh up-to-date beams for acquiring high SNR. Thanks to the full beam search, the highest beam SNR can be obtained. However, as illustrated in Fig. 6(b), it requires the highest power consumption of 27 dBm compared to the proposed EETBF of around 5 dBm. A slightly higher power of EETBF is required with higher transmission interval in order to obtain higher SNR to compromise high latency, as depicted in Fig. 6(c). Additionally, as shown in Fig. 6(c), the baseline scheme has the highest beam training latency of 16 ms. We can also observe that the proposed EETBF results in higher latency with the increment of transmission intervals, which is the result that more beams are required to retrain beamforming due to the out-of-date historical beam data. Combining Figs. 6(a) to 6(c) provides the total result of EE in Fig. 6(d). We can infer that it reaches the optimal transmission interval of 0.5 s for pedestrian velocity. This is because frequent beam training consumes more energy compared to longer transmission interval, whilst high latency and low SNR metrics dominate longer transmission interval. However, more beams and power are required for training, which results in a decreasing EE. Although the optimal beam can be obtained by the full beam search, its comparatively higher power consumption and beam training latency provoke

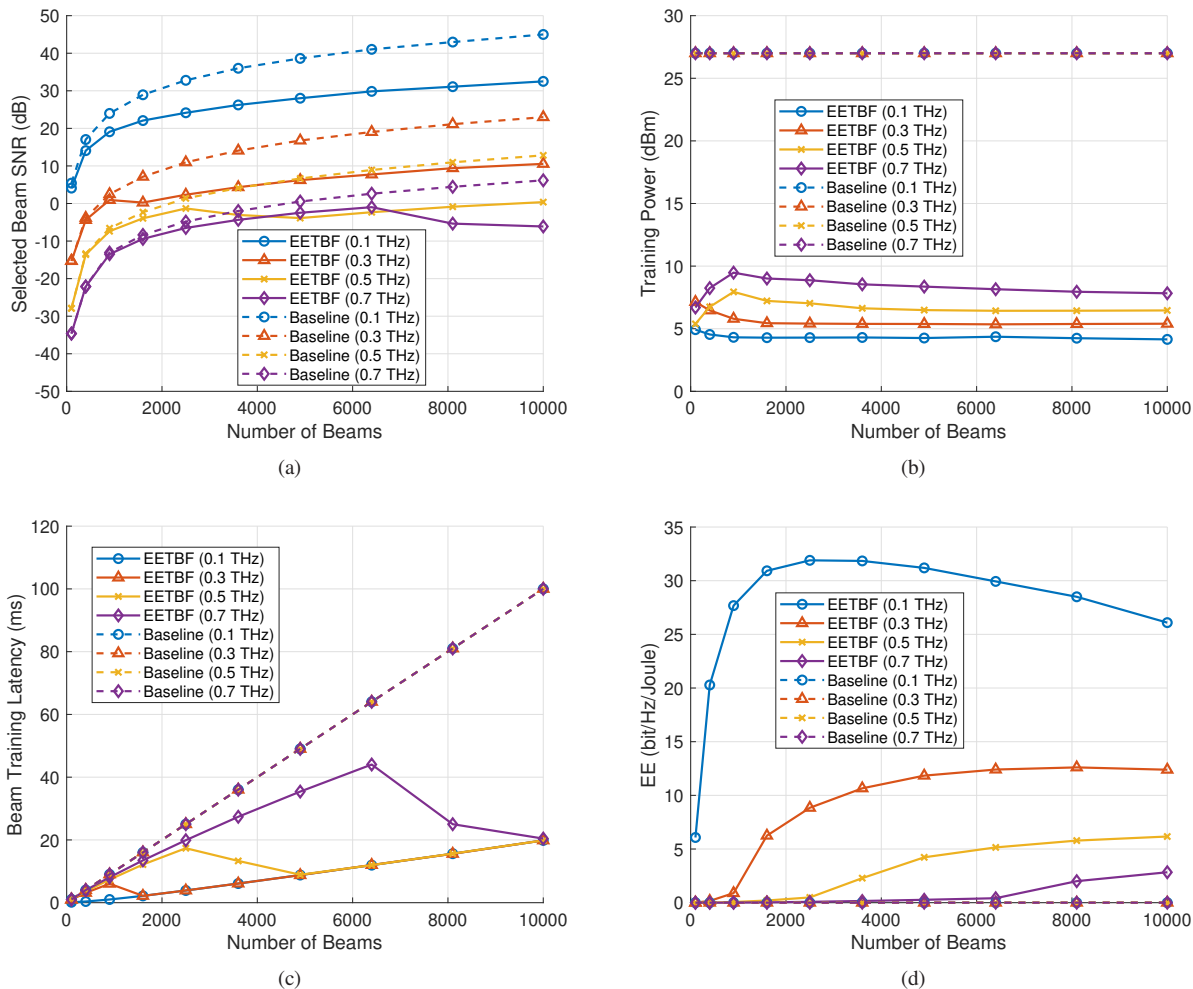


Fig. 7. Performance of EETBF compared to the baseline w.r.t. different frequencies of $\{0.1, 0.3, 0.5, 0.7\}$ THz and numbers of beams $[100, 10000]$. (a) Beam SNR (b) Training power (c) Training latency (d) EE.

the near zero EE.

C. Impact of Operating THz Bands

In Fig. 7, we study the performance of EETBF and compare it with the baseline scheme, when different frequencies of $\{0.1, 0.3, 0.5, 0.7\}$ THz and numbers of beams $[100, 10000]$ are considered. Note that a larger number of beams correspond to a smaller beamwidth, which can refer to Fig. 4. In Fig. 7(a), we can know that in most cases, more beams can achieve a higher SNR due to its higher degree of freedom of beam training. Nevertheless, with the increase of the number of beams at high frequency bands, lower SNR obtained may be affected by reduced training power and high latency, due to the fact that more beams are required to be trained for achieving high EE. As a result, we can see different trends of EETBF from Fig. 7(b). In Fig. 7(b), with a higher operating frequency of 0.7 THz, it consumes more power to train fewer beams to compensate high pathloss, but with less power for enormous beams to compromise high training latency. By contrast, the frequencies of $\{0.1, 0.3\}$ THz with lower pathloss can use more power to obtain high-quality beams with low latency. Observing from Fig. 7(c), we have intriguingly

turning points when $\{900, 2500, 6400\}$ beams at frequencies of $\{0.3, 0.5, 0.7\}$ THz, respectively. This is because it tends to sacrifice some training beams in exchange of more data transmission time even a low-SNR beam is obtained. Another turning points can be found when there are $\{1600, 4900\}$ beams at frequencies of $\{0.3, 0.5\}$ THz, respectively. With lower training power consumed, more beams are still required to obtain a moderate SNR. In Fig. 7(d), we can know that the baseline scheme attains nearly zero EE due to the high power and the linearly increasing latency. The compellingly low beam SNR dominates the result at higher THz frequencies even with low latency, leading to near zero EE. This implies that more beams are needed to generate high-SNR beams to compensate for the substantially high THz pathloss. However, under the modest pathloss, the EE performance curve of proposed EETBF has a concave characteristic with an optimal number of beams at 0.1 THz, owing to the fact that our EETBF can strike a compelling tradeoff between beam SNR, training power and training latency.

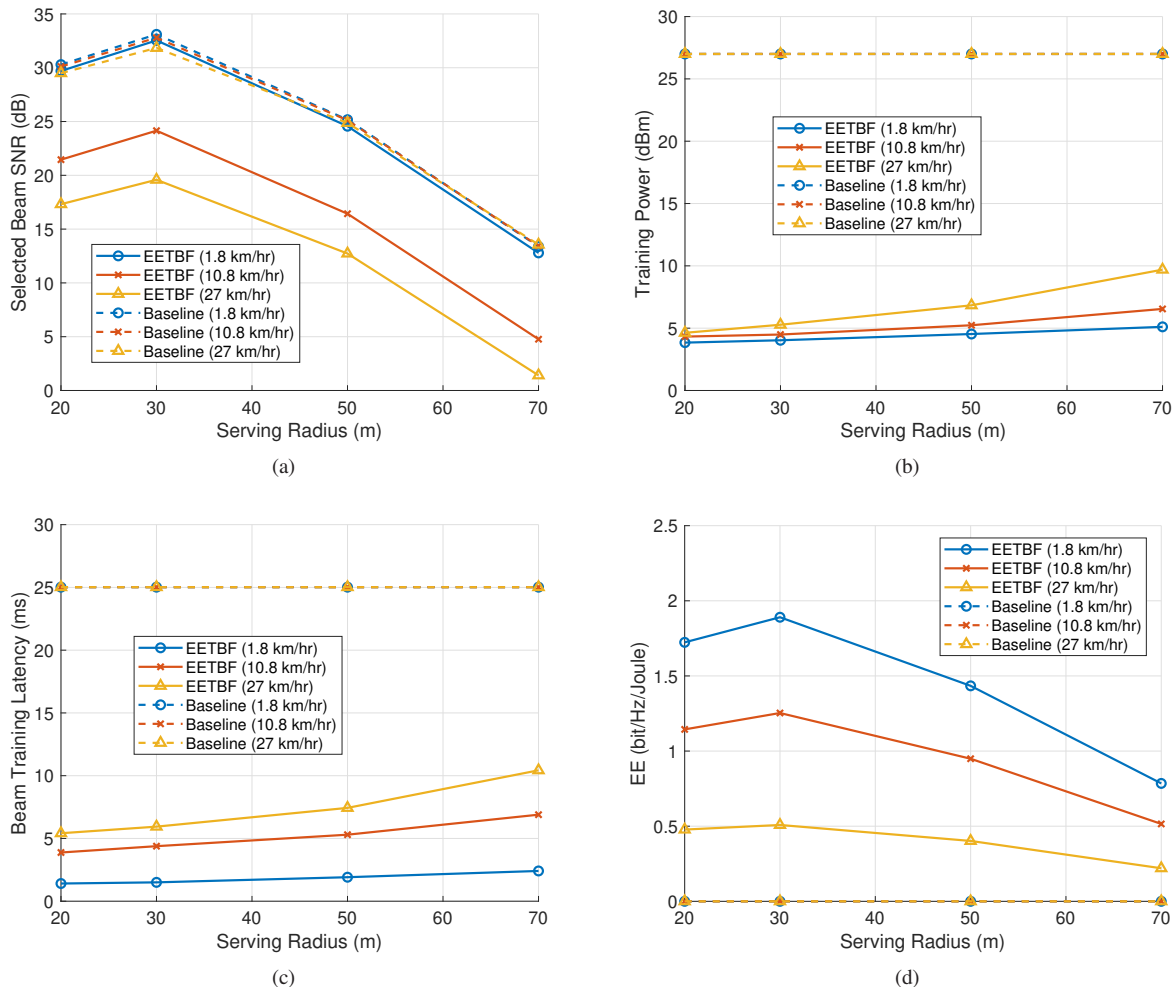


Fig. 8. Performance of EETBF compared to the baseline w.r.t. velocity values of $\{1.8, 10.8, 27\}$ km/hr and serving radius of $[20, 70]$ m. (a) Beam SNR (b) Training power (c) Training latency (d) EE.

D. Serving Radius

In Fig. 8, we evaluate the performance of EETBF and compare it with the performance of the baseline scheme, when different frequencies of $\{0.1, 0.3, 0.5, 0.7\}$ THz and serving radius of $[20, 70]$ m are considered. In Fig. 8(a), we can observe that there exists an optimal serving radius of about 30 m for all cases. When the serving radius is below 30 m, more power and more training beams are leveraged to obtain a higher beam SNR. On the contrary, when the serving radius is more than 30 m, the substantial pathloss dominates the result, leading to a lower beam SNR even when much more power and many beams for training are used. Accordingly, the EE has the asymptotic curves as that of beam SNR, and the optimal EE can be obtained when the serving radius is about 30 m.

E. Effect of Power Control

In Fig. 9, we compare the proposed EETBF scheme with and without PA mechanism as well as the baseline scheme at the velocity of $\{1.8, 10.8\}$ km/hr and the different numbers of beams of $[100, 10000]$. We can observe from Fig. 9(a) that the schemes with power control attain a lower beam

SNR in exchange for preserving more power as depicted Fig. 9(b). However, it consumes more power at higher velocity to compromise the low SNR. Owing to the high latency induced from full beam search, the training power of the baseline scheme with power control is declined in order to preserve power resources. Moreover, the training power of EETBF presents the convex curve shape. Less power is utilized for attaining higher EE with increasing numbers of beams, whereas more power is required to train more beams. Therefore, as illustrated in Fig. 9(c), the EETBF with power control has a slightly higher latency compared to that with full power utilization. In Fig. 9(d), we can see that the EETBF with power control achieves the highest EE, which is about three times higher than that of the EETBF without power control. By contrast, even the baseline scheme makes use of power conservation, it still provokes zero rate as well as zero EE due to the compellingly high beam training latency.

F. Benchmark Comparison

In Table II, we compare the proposed EETBF scheme with some existing methods in open literature, including the conventional exhaustive beam training [7], [30], random

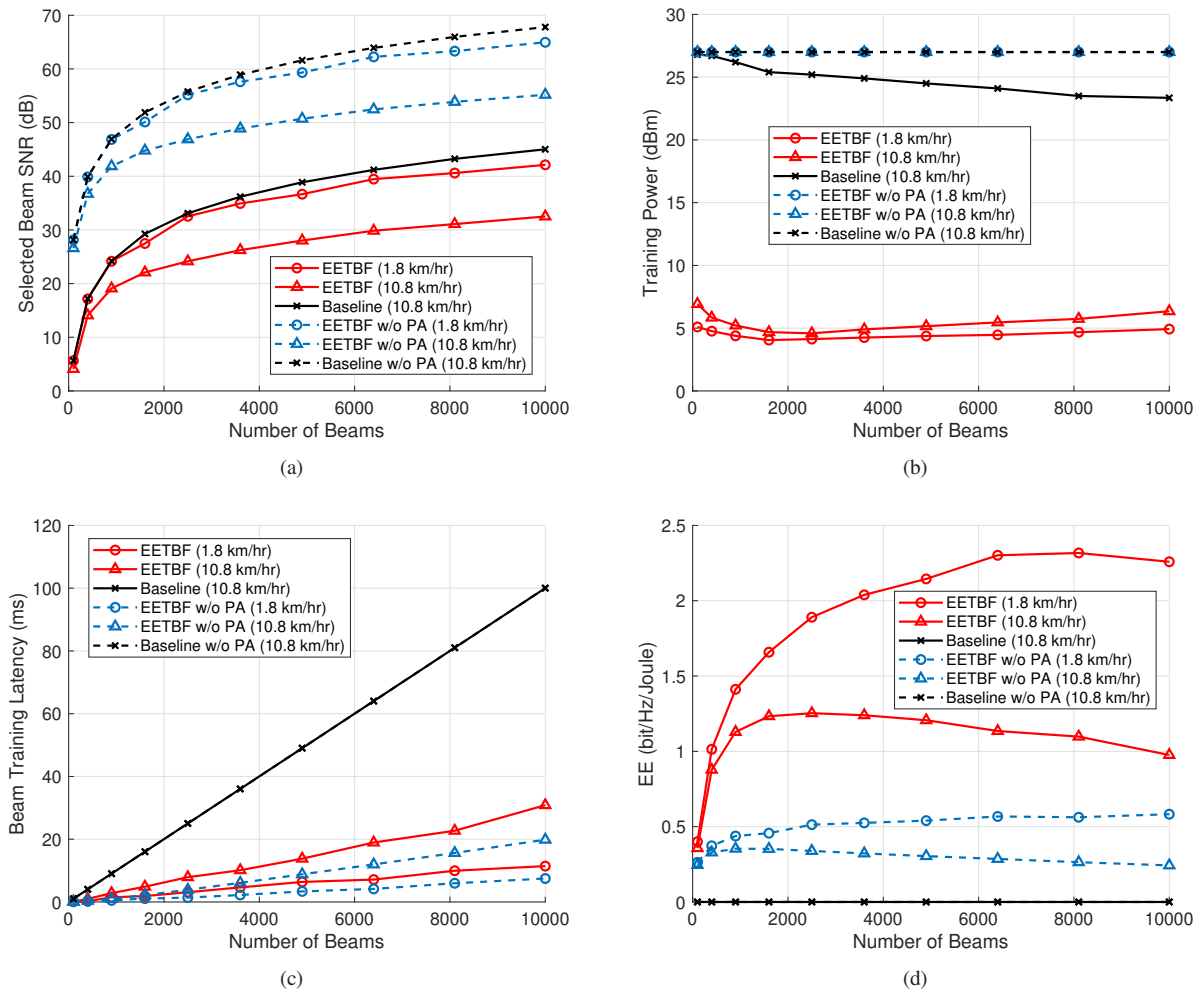


Fig. 9. Comparison of EETBF compared to that without PA mechanism and the baseline under different velocity values of {1.8, 10.8} and numbers of beams [100, 10000]. (a) Beam SNR (b) Training power (c) Training latency (d) EE.

TABLE II
BENCHMARK COMPARISON

	Protocol or Framework	Feedback Required	THz/mmWave Compatibility	Latency (ms)	SNR (dB)	Rate (bps/Hz)	Power (dBm)	EE (bit/Hz/Joule)
Proposed EETBF	This work	Once	THz	5	25	7.5	<8	2
Proposed EETBF w/o PA Mechanism			THz	5	40	12	27 (Max)	0.5
Exh. w/ PA	802.15.3d [7]		Both	>50	30	~0	<8	~0
Exh. w/o PA	802.11ad/ay [30]		Both	>50	50	~0	27 (Max)	~0
Random Search (~1000 beams)	Arbitrary		Both	10	10	3	27 (Max)	0.1
Iterative Search	802.15.3d [26] 802.11ad [32]	Per beam	Both	15	25	6	27 (Max)	0.2
Iterative Search (Power Control)			THz	10	20	5	>27	0.15
Linear Search	802.15.3c [38]		mmWave	35	20	2	27 (Max)	0.07
Binary search			mmWave	20	25	4	27 (Max)	0.15

beam search, iterative search [26], [32] and the linear/binary search methods [38]. In random search, we randomly select around 1000 beams for training. The iterative search employs a tree-based approach, starting with the largest candidate

beamwidth and progressively reducing the beamwidth. Furthermore, both linear and binary search methods utilize a fixed beamwidth. Linear search trains the consecutive neighboring beams, whereas binary search selects the intersecting beam

sectors. The corresponding adopted protocols of benchmarks for implementation are also listed in Table II. We can observe that the proposed EETBF as well as the exhaustive/random search require only a single feedback, which is carried out after all the training beams from BS are received. These are applicable in IEEE 802.11ad/ay frameworks and protocols. However, the mechanisms in [26], [32], [38] require frequent beam reports, which potentially lead to much higher training latency compared to the proposed scheme. Such methods are applicable for per-beam feedback based IEEE 802.15.3c or 802.15.3d frameworks and protocols. Theoretically, per-beam feedback has around twice the latency of single feedback. For instance, the EETBF has a latency of about 5 ms, whilst the linear and binary search have the respective latency of about 35 ms and 20 ms. Moreover, with the compellingly high latency induced by full beam search, no data transmission interval is left, leading to nearly zero rate as well as EE performance. Although high-SNR beams can be obtained through full power utilization, the EETBF without PA has an EE of only 0.5 bit/Hz/Joule. We further notice that the iterative search requires power higher than the maximum allowable power threshold, as it commences its training with wider beamwidths. In other words, much more power should be used to compensate for the lower beam gain at the beginning of the training; otherwise, no beams will be obtained. However, the proposed EETBF utilizes equal small beamwidths for beam training, which alleviates the issue. Moreover, the high latency of both linear and binary search methods is attained owing to the miscellaneous beam training and excessive feedbacks. To conclude, the proposed EETBF with PA can compromise the tradeoff between effective rate and power consumption, resulting in the highest EE of 2 bit/Hz/Joule.

V. CONCLUSIONS AND FUTURE WORKS

A. Conclusion Remarks

In this work, we have conceived a joint EE-oriented THz 3D beamforming training, which includes the EETBF-BT for beam training and the EETBF-PA for power control. Owing to the high pathloss at THz frequencies, our EETBF is capable of striking a compelling tradeoff between the beamforming gain and power consumption for achieving the highest EE performance. Simulation results have revealed the optimal configurations of the transmission interval, number of beams as well as the serving radius under various user's moving velocities and frequency bands. The studies and results have shown that the proposed EETBF outperforms the existing benchmarks of leveraging full beam search, iterative search, linear/binary search as well as the non-power-control based mechanism found in open literature. The proposed EETBF can achieve the lowest training latency and power consumption, resulting in the highest effective rate and EE performance.

B. Challenges and Future Works

Here, we provide the potential challenges and real-world feasibility of implementing EETBF in existing THz communication systems. First, a more practical beamforming model can be considered, which may affect the 3D beamforming

gain and its alignment. The uncertain misalignment will affect the training policy, especially under high mobility scenarios, potentially leading to lost feedback information. Second, out-of-band frequency utilization can be adopted to significantly enhance the training efficiency. For example, beam training using hybrid bands in sub-6 GHz or mmWave bands can transfer their partial knowledge to THz bands. However, such a mechanism might complicate the framework and protocol, which can be regarded as an open research. Third, existing architectures allow the BS to control its power in different sub-channels or sub-carriers mostly only for data transfer. Therefore, BS requires more complex power control for each training beam and data beam in EETBF. To elaborate a little further, we can also regard the proposed framework and EETBF as a general mechanism for compromising single- and per-beam based feedback. As an extension, training performance can be improved by appropriately adjusting the total frame interval and the number of training beams as well as of feedbacks based on the dynamic environments. Such framework requires a more complex algorithm and protocol, which can be left as the future promising work.

REFERENCES

- [1] Z. Zhang, Y. Xiao, Z. Ma, M. Xiao, Z. Ding, X. Lei, G. K. Karagiannidis, and P. Fan, "6G wireless networks: Vision, requirements, architecture, and key technologies," *IEEE Vehicular Technology Magazine*, vol. 14, no. 3, pp. 28–41, 2019.
- [2] I. F. Akyildiz, A. Kak, and S. Nie, "6G and beyond: The future of wireless communications systems," *IEEE Access*, vol. 8, pp. 133 995–134 030, 2020.
- [3] L.-H. Shen, K.-T. Feng, and L. Hanzo, "Five facets of 6G: Research challenges and opportunities," *ACM Computing Surveys*, vol. 55, no. 11, pp. 1–39, 2023.
- [4] H. Elayan, O. Amin, B. Shihada, R. M. Shubair, and M.-S. Alouini, "Terahertz band: The last piece of RF spectrum puzzle for communication systems," *IEEE Open Journal of the Communications Society*, vol. 1, pp. 1–32, 2020.
- [5] Z. Chen, X. Ma, B. Zhang, Y. Zhang, Z. Niu, N. Kuang, W. Chen, L. Li, and S. Li, "A survey on terahertz communications," *China Communications*, vol. 16, no. 2, pp. 1–35, 2019.
- [6] Y. Jiang, G. Li, H. Ge, F. Wang, L. Li, X. Chen, M. Lu, and Y. Zhang, "Machine learning and application in terahertz technology: A review on achievements and future challenges," *IEEE Access*, vol. 10, pp. 53 761–53 776, 2022.
- [7] V. Petrov, T. Kurner, and I. Hosako, "IEEE 802.15.3d: First standardization efforts for sub-terahertz band communications toward 6G," *IEEE Communications Magazine*, vol. 58, no. 11, pp. 28–33, 2020.
- [8] M. T. Hossain and H. Tabassum, "Mobility-aware performance in hybrid rf and terahertz wireless networks," *IEEE Transactions on Communications*, vol. 70, no. 2, pp. 1376–1390, 2022.
- [9] K. Guan, G. Li, T. Kürner, A. F. Molisch, B. Peng, R. He, B. Hui, J. Kim, and Z. Zhong, "On millimeter wave and THz mobile radio channel for smart rail mobility," *IEEE Transactions on Vehicular Technology*, vol. 66, no. 7, pp. 5658–5674, 2017.
- [10] L. Zhang, Y.-C. Liang, and D. Niyato, "6G visions: Mobile ultra-broadband, super internet-of-things, and artificial intelligence," *China Communications*, vol. 16, no. 8, pp. 1–14, 2019.
- [11] L. Feng, Q. Yang, D. Park, and K. S. Kwak, "Energy efficient nano-node association and resource allocation for hierarchical nano-communication networks," *IEEE Transactions on Molecular, Biological and Multi-Scale Communications*, vol. 4, no. 4, pp. 208–220, 2018.
- [12] "Horizon 2020: The EU framework programme for research and innovation," European Union Horizon 2020 Research Program, 2020. [Online]. Available: <https://research-and-innovation.ec.europa.eu/funding/funding-opportunities/funding-pro>
- [13] H. Sarrideen, M.-S. Alouini, and T. Y. Al-Naffouri, "Terahertz-band ultra-massive spatial modulation MIMO," *IEEE Journal on Selected Areas in Communications*, vol. 37, no. 9, pp. 2040–2052, 2019.

- [14] A. Faisal, H. Sameddeen, H. Dahrouj, T. Y. Al-Naffouri, and M.-S. Alouini, "Ultramassive MIMO systems at terahertz bands: Prospects and challenges," *IEEE Vehicular Technology Magazine*, vol. 15, no. 4, pp. 33–42, 2020.
- [15] A. M. Elbir, K. V. Mishra, and S. Chatzinotas, "Terahertz-band joint ultra-massive MIMO radar-communications: Model-based and model-free hybrid beamforming," *IEEE Journal of Selected Topics in Signal Processing*, vol. 15, no. 6, pp. 1468–1483, 2021.
- [16] T. S. Rappaport, Y. Xing, O. Kanhere, S. Ju, A. Madanayake, S. Mandal, A. Alkhateeb, and G. C. Trichopoulos, "Wireless communications and applications above 100 GHz: Opportunities and challenges for 6G and beyond," *IEEE Access*, vol. 7, pp. 78 729–78 757, 2019.
- [17] J. M. Jornet and I. F. Akyildiz, "Channel modeling and capacity analysis for electromagnetic wireless nanonetworks in the terahertz band," *IEEE Transactions on Wireless Communications*, vol. 10, no. 10, pp. 3211–3221, 2011.
- [18] V. Petrov, J. Kokkonen, D. Moltchanov, J. Lehtomaki, Y. Koucheryav, and M. Juntti, "Last meter indoor terahertz wireless access: Performance insights and implementation roadmap," *IEEE Communications Magazine*, vol. 56, no. 6, pp. 158–165, 2018.
- [19] K. Tekbiyik, A. R. Ekti, G. K. Kurt, A. Gorcin, and H. Yanikomeroglu, "A holistic investigation of terahertz propagation and channel modeling toward vertical heterogeneous networks," *IEEE Communications Magazine*, vol. 58, no. 11, pp. 14–20, 2020.
- [20] I. F. Akyildiz, C. Han, and S. Nie, "Combating the distance problem in the millimeter wave and terahertz frequency bands," *IEEE Communications Magazine*, vol. 56, no. 6, pp. 102–108, 2018.
- [21] C. Lin and G. Y. Li, "Energy-efficient design of indoor mmWave and sub-THz systems with antenna arrays," *IEEE Transactions on Wireless Communications*, vol. 15, no. 7, pp. 4660–4672, 2016.
- [22] L. Feng, A. Ali, M. Iqbal, F. Ali, I. Raza, M. H. Siddiqi, M. Shafiq, and S. A. Hussain, "Dynamic wireless information and power transfer scheme for nano-empowered vehicular networks," *IEEE Transactions on Intelligent Transportation Systems*, vol. 22, no. 7, pp. 4088–4099, 2021.
- [23] H. Jiang, Y. Niu, B. Ai, Z. Zhong, and S. Mao, "QoS-aware bandwidth allocation and concurrent scheduling for terahertz wireless backhaul networks," *IEEE Access*, vol. 8, pp. 125 814–125 825, 2020.
- [24] H. Zhang, Y. Duan, K. Long, and V. C. M. Leung, "Energy efficient resource allocation in terahertz downlink NOMA systems," *IEEE Transactions on Communications*, vol. 69, no. 2, pp. 1375–1384, 2021.
- [25] C. Lin and G. Y. Li, "Adaptive beamforming with resource allocation for distance-aware multi-user indoor terahertz communications," *IEEE Transactions on Communications*, vol. 63, no. 8, pp. 2985–2995, 2015.
- [26] B. Ning, Z. Chen, W. Chen, Y. Du, and J. Fang, "Terahertz multi-user massive MIMO with intelligent reflecting surface: Beam training and hybrid beamforming," *IEEE Transactions on Vehicular Technology*, vol. 70, no. 2, pp. 1376–1393, 2021.
- [27] C. Huang, Z. Yang, G. C. Alexandropoulos, K. Xiong, L. Wei, C. Yuen, Z. Zhang, and M. Debbah, "Multi-hop RIS-empowered terahertz communications: A DRL-based hybrid beamforming design," *IEEE Journal on Selected Areas in Communications*, vol. 39, no. 6, pp. 1663–1677, 2021.
- [28] Z. Wan, Z. Gao, F. Gao, M. D. Renzo, and M.-S. Alouini, "Terahertz massive MIMO with holographic reconfigurable intelligent surfaces," *IEEE Transactions on Communications*, vol. 69, no. 7, pp. 4732–4750, 2021.
- [29] L.-H. Shen, K.-T. Feng, and L. Hanzo, "Coordinated multiple access point multiuser beamforming training protocol for millimeter wave WLANs," *IEEE Transactions on Vehicular Technology*, vol. 69, no. 11, pp. 13 875–13 889, 2020.
- [30] Y. Ghasempour, C. R. C. M. da Silva, C. Cordeiro, and E. W. Knightly, "Ieee 802.11ay: Next-generation 60 GHz communication for 100 gb/s Wi-Fi," *IEEE Communications Magazine*, vol. 55, no. 12, pp. 186–192, 2017.
- [31] B. Ning, Z. Chen, W. Chen, and Y. Du, "Channel estimation and transmission for intelligent reflecting surface assisted THz communications," in *Proc. IEEE International Conference on Communications (ICC)*, 2020, pp. 1–7.
- [32] J. Kim and A. F. Molisch, "Fast millimeter-wave beam training with receive beamforming," *Journal of Communications and Networks*, vol. 16, no. 5, pp. 512–522, 2014.
- [33] B. Ning, Z. Chen, Z. Tian, C. Han, and S. Li, "A unified 3D beam training and tracking procedure for terahertz communication," *IEEE Transactions on Wireless Communications*, pp. 1–1, 2021.
- [34] A. Ahmadi and O. Semiari, "Reinforcement learning for optimized beam training in multi-hop terahertz communications," in *Proc. IEEE International Conference on Communications (ICC)*, 2021, pp. 1–6.
- [35] J. Tan and L. Dai, "Wideband beam tracking in THz massive MIMO systems," *IEEE Journal on Selected Areas in Communications*, vol. 39, no. 6, pp. 1693–1710, 2021.
- [36] L.-H. Shen, T.-W. Chang, K.-T. Feng, and P.-T. Huang, "Design and implementation for deep learning based adjustable beamforming training for millimeter wave communication systems," *IEEE Transactions on Vehicular Technology*, vol. 70, no. 3, pp. 2413–2427, 2021.
- [37] T.-W. Chang, L.-H. Shen, and K.-T. Feng, "Learning-based beam training algorithms for IEEE 802.11ad/ay networks," in *Proc. IEEE Vehicular Technology Conference (VTC-Spring)*, 2019, pp. 1–5.
- [38] Y. Yaman and P. Spasojevic, "Reducing the LOS ray beamforming setup time for IEEE 802.11ad and IEEE 802.15.3c," in *Proc. IEEE Military Communications Conference (MILCOM)*, 2016, pp. 448–453.
- [39] L.-H. Shen, Y.-C. Chen, and K.-T. Feng, "Mobility-aware fast beam training scheme for IEEE 802.11ad/ay wireless systems," in *Proc. IEEE Wireless Communications and Networking Conference (WCNC)*, 2018, pp. 1–6.
- [40] N. C. Luong, D. T. Hoang, S. Gong, D. Niyato, P. Wang, Y.-C. Liang, and D. I. Kim, "Applications of deep reinforcement learning in communications and networking: A survey," *IEEE Communications Surveys Tutorials*, vol. 21, no. 4, pp. 3133–3174, 2019.
- [41] M. Chen, U. Challita, W. Saad, C. Yin, and M. Debbah, "Artificial neural networks-based machine learning for wireless networks: A tutorial," *IEEE Communications Surveys Tutorials*, vol. 21, no. 4, pp. 3039–3071, 2019.
- [42] L.-H. Shen, K.-T. Feng, T.-S. Lee, Y.-C. Lin, S.-C. Lin, C.-C. Chang, and S.-F. Chang, "AI-enabled unmanned vehicle-assisted reconfigurable intelligent surfaces: Deployment, prototyping, experiments, and opportunities," *IEEE Network*, vol. 38, no. 6, pp. 289–299, 2024.
- [43] P.-C. Hsu, L.-H. Shen, C.-H. Liu, and K.-T. Feng, "Federated deep reinforcement learning for THz-beam search with limited CSI," in *Proc. IEEE Vehicular Technology Conference (VTC-Fall)*, 2022, pp. 1–6.
- [44] R. Sutton and A. Barto, "Reinforcement learning: An introduction," *IEEE Transactions on Neural Networks*, vol. 9, no. 5, pp. 1054–1054, 1998.